Investigating spin-transfer torques induced by thermal gradients in magnetic tunnel junctions by using micro-cavity ferromagnetic resonance

Cansever, H.; Narkowicz, R.; Lenz, K.; Fowley, C.; Ramasubramanian, L.; Yildirim, O.; Niesen, A.; Huebner, T.; Reiss, G.; Lindner, J.; Fassbender, J.; Deac, A. M.;

Originally published:

May 2018

Journal of Physics D: Applied Physics 51(2018), 224009

DOI: https://doi.org/10.1088/1361-6463/aac03d

J. Phys. D: Appl. Phys. **00** (2018) 000000 (10pp)

Investigating spin-transfer torques induced by thermal gradients in magnetic tunnel junctions by using micro-cavity ferromagnetic resonance

H Cansever[1,2], R Narkowicz[1], K Lenz[1], C Fowley[1], L Ramasubramanian[1], O Yildirim[3], A Niesen[4], T Huebner[4], G Reiss[4], J Lindner[1], J Fassbender[1,2] and A M Deac[1]

[1] Helmholtz-Zentrum Dresden—Rossendorf, Institute of Ion Beam Physics and Materials Research, Bautzner Landstraße 400, 01328 Dresden, Germany
[2] Technische Universität Dresden, Institute of Solid State Physics, 01069 Dresden, Germany
[3] Empa-Swiss Federal Laboratories for Materials Science and Technology, 8600 Dübendorf, Switzerland
[4] Department of Physics, Center for Spinelectronic Materials and Devices, Bielefeld University, 33615 Bielefeld, Germany

E-mail: xxxx

Received 31 December 2017, revised 23 March 2018
Accepted for publication 26 April 2018
Published

Abstract

Similar to electrical currents flowing through magnetic multilayers, thermal gradients applied across the barrier of a magnetic tunnel junction may induce pure spin-currents and generate 'thermal' spin-transfer torques large enough to induce magnetization dynamics in the free layer. In this study, we describe a novel experimental approach to observe spin-transfer torques induced by thermal gradients in magnetic multilayers by studying investigating in their ferromagnetic resonance response by using microresonator cavities. Utilizing this approach allows for measuring micron/nano-sized samples in order to detect magnetization dynamics in open-circuit conditions, i.e. without the need of electrical contacts. We performed first experiments on magnetic tunnel junctions patterned into $6 \times 9\ \mu m^2$ ellipses from Co_2FeAl/MgO/CoFeB stacks. We conducted microresonator ferromagnetic resonance (FMR) under focused laser illumination to induce thermal gradients in the layer stack and compared them to measurements in which the sample was globally heated from the backside of the substrate. Moreover, we carried out broadband FMR measurements under global heating conditions on the same extended films the microstructures were later on prepared from. The results clearly demonstrate the effect of thermal spin-torque on the FMR response and thus show that the microresonator approach is well suited to investigate thermal spin-transfer driven processes for small temperatures gradients, far from being sufficient for magnetic switching.

Keywords: thermal spin transfer torque, microresonator, ferromagnetic resonance, magnetic tunnel junction

(Some figures may appear in colour only in the online journal)

1. Introduction

Spin caloritronics is a new research area which investigates the non-equilibrium generation of spin-currents by thermal gradients and their interaction with magnetic moments [1, 2].

The field of thermoelectrics dates back to the discovery of the Seebeck effect in 1821. The Seebeck effect is a thermoelectric phenomenon describing the fact that between two points of a conductor that exhibit different temperatures an electrical voltage develops, due to the temperature driven

JNL:JPD PIPS: AAC03D TYPE: SPE TS: NEWGEN DATE:3/5/18 EDITOR: IOP SPELLING: US

diffusion processes of the electrons. The ratio of voltage-to-temperature difference is called Seebeck coefficent. In order to make use of this voltage, two conductors with different Seebeck coefficients have to be connected, leading to a device called 'thermocouple'. A thermocouple allows for measuring temperature differences between two contact locations of different conducting materials via the generated thermo-voltage[5]. More recently, it has been theoretically predicted and experimentally demonstrated that a temperature gradient within a ferromagnet can induce what is called spin-Seebeck effect [3]. As the exchange interaction generates two different electronic spin-channels ('spin-up' and 'spin-down'), both types of electrons exhibit different Seebeck-coefficients and thus different temperature-driven diffusion properties. A ferromagnet under the influence of a thermal gradient develops a spin-accumulation (imbalance of 'spin-up' and 'spin-down' electrons along the gradient) that can be analogously described as 'spin-voltage' that drives a spin-current along the gradient.

While the first experimental detection of a spin-current generated by the spin-Seebeck effect was performed via the inverse spin-Hall effect in a non-ferromagnetic metal adjacent to a ferromagnet [3], effects in more complex layer stacks were explored in follow-up studies. In this context we mention tunneling between two magnetic layers separated by an insulator (magneto-Seebeck effect) [2], as well as spin-injection from a ferromagnet to a semiconductor (spin-Seebeck tunneling) [4].

Exploring potential applications, Hatami *et al* theoretically studied the spin-Seebeck effect in spin-valves and introduced the concept of thermal spin-transfer torques (T-STT). They predicted that the thermally induced spin-current creates an spin-imbalance at the interface between non-magnetic and ferromagnetic layers [5], thus causing a transfer of spin angular momentum across the non-magnetic spacer and exerting a torque on the local magnetization of the ferromagnetic layer. Experimentally, T-STT were studied within asymmetric Co/Cu/Co nanowire spin-valves which exhibit switching field changes under varying a.c. currents causing Joule heating [6]. It was also theoretically predicted that temperature differences of around 10 K across an ultrathin barrier (1 nm) can create magnetization dynamics in Fe/MgO/Fe magnetic tunnel junctions [7]. The authors reported that T-STT exhibit asymmetric angular dependencies, unlike torques induced by electrical bias. Thermal gradients (ΔT) of 6.5 K and 56.5 K were predicted to even induce switching from the antiparallel (AP) to the parallel state (P) and vice-versa, respectively. In addition, it was pointed out that the crystalline quality of the tunnel barrier is crucial, directly affecting the magnitude of thermal torques [7]. The spin-Seebeck effect has been studied on CoFeB/MgO/CoFeB magnetic tunnel junctions, using different heating methods such as Joule heating, heating with Peltier elements, as well as laser heating [8–14]. Most results are supported by finite element simulations that predict temperature gradients across the MgO barrier in the order of a few mK. In order to increase the thermal gradients across the barrier, $MgAl_2O_4$ layers were used as tunnel barriers in magnetic tunnel junctions, due to their lower thermal conductivity as compared to MgO barriers [14]. It was reported that magnetic layers separated by a $MgAl_2O_4$ barrier exhibit a higher tunneling magneto Seebeck (TMS) ratio. Recently, T-STT have been studied on MgO-based magnetic tunnel junctions by using electrically detected ferromagnetic resonance (FMR) techniques [15]. The changes on the FMR line-shape were determined by the ratio of dispersive (D) and absorptive (L) components (D/L) of the spectra. This D/L ratio increases under thermal gradients due to T-STT. It was also found that the angular dependence of D/L exhibited different behavior than the current driven STT.

In this study, we describe a different approach, which focuses on observing and quantifying spin-transfer torques induced by thermal gradients in magnetic multilayers without electrical contacts, analyzing changes in their FMR response under laser heating. To access the FMR response of micron-size devices, micro-cavity resonators (also referred to as microresonators) were fabricated around the MTJs.

1.1. Thermal spin-transfer torques

Similar to electrical currents flowing through magnetic multilayers that become spin-polarized and consequently transfer angular momentum to the magnetic moments of subsequent layers [27, 28], it has been predicted that thermal gradients applied across the spacer of a spin-valve or a magnetic tunnel junction may induce pure spin-currents and generate 'thermal' spin-transfer torques (T-STTs) large enough to induce magnetization dynamics [5, 7]. The relation of spin-current, charge current and heat current was theoretically described by Bauer *et al* using Onsager's reciprocity rule [2, 29]. In fact, spin-currents can be driven not only by gradients of the electrochemical potential (i.e. by bias voltages), but also by thermal gradients. It was shown in [5] that the spin-torque resulting from spin-currents due to the presence of a bias voltage ΔV, in addition to thermal gradient ΔT across the sample stack, is given by $\tau \sim (P\Delta V + P'S\Delta \mathrm{T})$. Here, $P = \left(G^{\uparrow} - G^{\downarrow}\right)/(G^{\uparrow} + G^{\downarrow})$ is the polarization of the conductance, with $|P| \leqslant 1$, P' is the polarization of its energy derivative at the Fermi level and S is the Seebeck coefficient. In this respect, the quantity P describes the spin assymetry of the electrical conductivity and P' describes the spin assymetry of the Seebeck coefficient. While P ist fundamentally limited in magnitude, $P'S$ can be very large and, consequently, spin-transfer processes due to thermal gradients are of high interest. The spin-transfer torque mechanism is schematically depicted in figure 1. Here $\mathbf{m_r}$ and $\mathbf{m_f}$ represent magnetic unit vectors of the reference and the free layer, respectively. $\boldsymbol{T}_{\parallel}$ and $\boldsymbol{T}_{\perp}$ are the in-plane and perpendicular spin-transfer torques[6], which can be generated by the bias voltages or thermal gradients, respectively.

In general, magnetization dynamics can be described by the Landau–Lifshitz—Gilbert equation, and can be detected experimentally by measuring FMR [30].

[5] Note that in case the voltage is tried to be picked up at the two ends of the conductor itself by means of a measurement device, the overall voltage will cancel to zero.

[6] Note that here 'in-plane' and 'perpendicular' refer to the plane defined by the magnetic moments of the free and the reference layers.

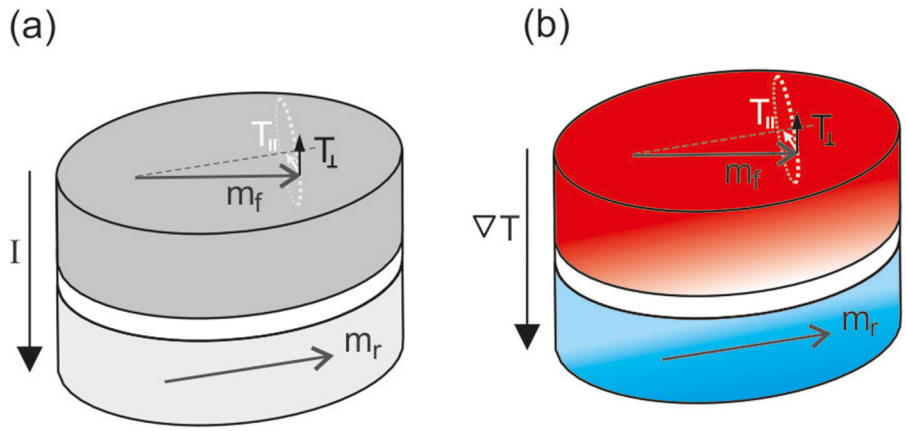

Figure 1. Sketch of spin-transfer torque induced (a) by bias voltage and (b) by thermal gradient.

$$\frac{d\boldsymbol{m}_f}{dt} = -\gamma \boldsymbol{m}_f \times \boldsymbol{B}_{eff} + \alpha \boldsymbol{m}_f \times \frac{d\boldsymbol{m}_f}{dt}. \quad (1)$$

Here, γ is the gyromagnetic ratio, α is the damping factor and $\boldsymbol{B}_{eff}$ is the effective magnetic field, which in general may include demagnetization, applied and anisotropy fields. The effect of spin-currents is described by two extra terms [27, 37]:

$$\begin{aligned}\frac{d\boldsymbol{m}_f}{dt} = &-\gamma \boldsymbol{m}_f \times \boldsymbol{B}_{eff} + \alpha \boldsymbol{m}_f \times \frac{d\boldsymbol{m}_f}{dt} \\ &+ \gamma T_{\parallel} \left[\boldsymbol{m}_f \times (\boldsymbol{m}_f \times \boldsymbol{m}_r)\right] + \gamma T_{\perp} (\boldsymbol{m}_f \times \boldsymbol{m}_r)\end{aligned} \quad (2)$$

where $T_{\parallel}$ and $T_{\perp}$ are the magnitudes of the in-plane and perpendicular spin-torque, respectively. The in-plane spin-torque term is written as a double cross product between the magnetization and direction of the polarization of the spin-current (assumed to be parallel to the reference layer). It is also called damping-like term, as it is mathematically similarly written as the damping term in the Landau–Lifshitz form. The fourth term is written as a simple cross product between the two vectors; hence it is referred to as 'perpendicular' or 'field-like' spin-torque term. It was also shown that the perpendicular component of the spin-torque effects the output frequency of thermally-excited FMR signals in MgO-based magnetic tunnel junctions, while the in-plane component changes their linewidth [31].

2. Experimental details

2.1. Ferromagnetic resonance detection using microresonators

FMR is commonly used to obtain information about magnetic anisotropy, g-factor, and damping parameters of ferromagnetic materials [16–20]. In FMR experiments, the magnetic layers are excited by microwave fields at fixed frequency, while a d.c. magnetic field is swept through the resonance. A microwave generator supplies the required power, while an electromagnet is used to create a slowly varying homogenous magnetic field in the sample volume, which can be safely assumed to be static on the timescale of the magnetic resonance precession frequency.

A microwave bridge in combination with field-modulation and lock-in technique is commonly used in order to improve the detection sensitivity (figure 2) [21]. One part of the microwave power is coupled into the excitation arm of the spectrometer, where the power level can be adjusted by an attenuator and finally is launched via the circulator into the resonant cavity, which is almost perfectly matched to the input line at its resonance frequency. The other (main) part of the power is sent into the reference arm and biases the quadrature mixer at the operation frequency (homodyne detector). The phase shifter in the reference arm allows for adjustment of the phase at the local oscillator (LO) input of the quadrature mixer. It is thus possible to detect the absorption and dispersion FMR signals on the I and Q outputs respectively, as they are phase–shifted by 90°.

At external magnetic fields off resonance, the power reflected by the cavity remains negligible and only when the resonance condition is met, a strong change of the magnetic susceptibility of the sample leads to a change of the resonator's impedance, and consequently to an increased reflection of microwave power. The reflected signal is conducted via the circulator to the detection arm, where a low noise preamplifier amplifies both signal and noise. As a result, the thermal noise of the cavity dominates other possible sources of noise and determines the noise level of the whole setup. The amplified signal is fed to the radio-frequency (RF) input of the mixer and down-converted at the same operation frequency[7]. This homodyne down-conversion scheme is highly selective for the weak signals on the noise background.

[7] The mixer multiplies the signals $u_{RF}(t) = f(t)\cos[\omega_{RF}t]$ (with f(t) being a time dependence varying slowly on the time-scale set by ω_{RF}) and $u_{LO}(t) = A_{LO}\cos[\omega_{LO}t]$ which—via the trigonometric relation $\cos A \cos B = \frac{1}{2}[\cos(A+B) + \cos(A-B)]$—yields $u_{out}(t) = u_{LO}(t) \cdot u_{RF}(t) = \frac{A_{LO} \cdot f(t)}{2}\{\cos[(\omega_{RF} + \omega_{LO})t] + \cos[(\omega_{RF} - \omega_{LO})t]\}$. After low-pass filtering, one ends up with a signal that is given by $u_{out}(t) = \frac{A_{LO} \cdot f(t)}{2} \cdot \cos[(\omega_{RF} - \omega_{LO})t]$. In case that $\omega_{RF} \approx \omega_{LO}$ (homodyne detection), one ends up with $u_{out}(t) = \frac{A_{LO} \cdot f(t)}{2}$ which is the signal to be detected with the lock-in amplifier.

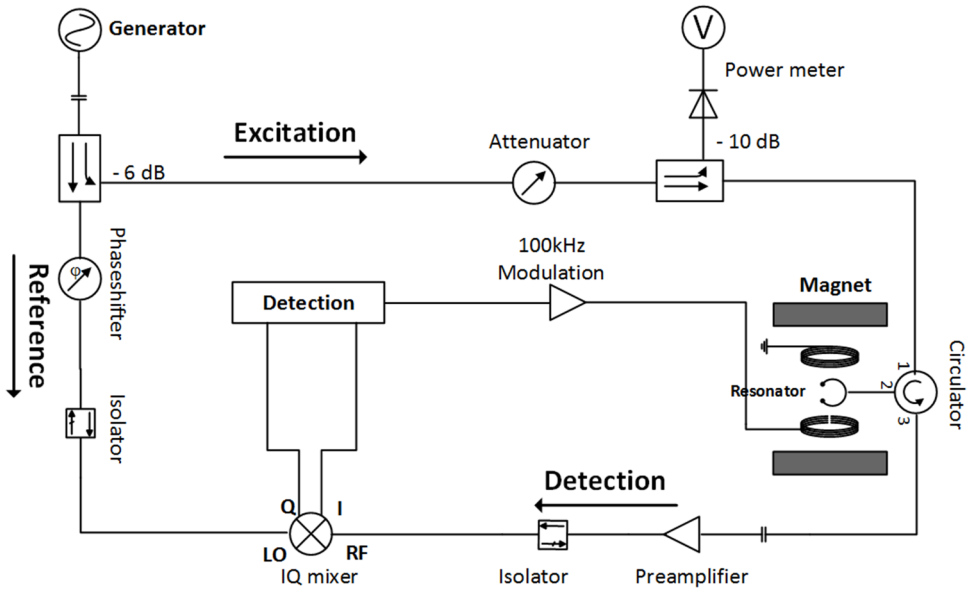

Figure 2. Schematic of the FMR spectrometer. Following microwave parts are used in the microwave bridge: generator APSIN20G (AnaPico), −6 dB and −10 dB directional couplers 1815 and 1822 (Krytar), attenuator AF885H-20 (ATM), phase shifter 6705-2 (API), power meter U8487A-RF (Keysight), circulator—K70-1FFF—and isolators K70-1LFF (Aerotek), preamplifier BZT-06001800-151030-172320 (B&Z Technologies), quadrature mixer IQ0318L (Marki Microwave). For signal detection a lock-in amplifier 7270 (Ametek) is used.

To further increase the sensitivity, a phase-sensitive detection is used. The static magnetic field is modulated at the frequency where the noise floor is determined by thermal noise, usually about 100 kHz. This frequency is significantly lower than the FMR frequency. Hence, the frequency modulation at 100 kHz will pass the LO and RF input of the quadrature mixer, without influence. The low-frequency magnetic field modulation encodes spectral information on the microwave signal. Lock-in detection at the I output of the quadrature mixer is only sensitive to signals that have the same frequency and phase as the field modulation and extracts a signal resembling the derivative of a Lorentzian absorption curve as shown in figure 3. The Q output of the mixer delivers the derivative of the dispersion signal that will not be registered in our measurements throughout this paper. The equivalent noise bandwidth of such a detection scheme can be further reduced by setting an appropriate lock-in integration constant.

The amplitude of the FMR signal measured in such a spectrometer is determined not only by the change of the sample magnetization but also by the resonator used for the FMR detection [33]:

$$U_{sig} \approx \frac{\partial \chi''}{\mu_0 \partial H} F Q_L, \tag{3}$$

here $\partial\chi''/\partial H$ is the derivative of the imaginary part of the magnetic high frequency susceptibility, F is the filling factor and $Q_L = 2\pi \frac{W_{\text{cav}}^{\text{store}}}{W_{\text{loss}}^{\text{int}} + W_{\text{loss}}^{\text{ext}}}$ is the loaded quality factor of the resonator which describes the ratio of the energy stored in the cavity at its resonance frequency $W_{\text{cav}}^{\text{store}}$ to the sum of the energy losses per cycle inside the cavity $\left(W_{\text{loss}}^{\text{int}}\right)$ and the external losses due to reflection at the coupler (coupling hole or antenna) and dissipation into the matched load of the generator $\left(W_{\text{loss}}^{\text{ext}}\right)$[8]. The filling factor is defined by,

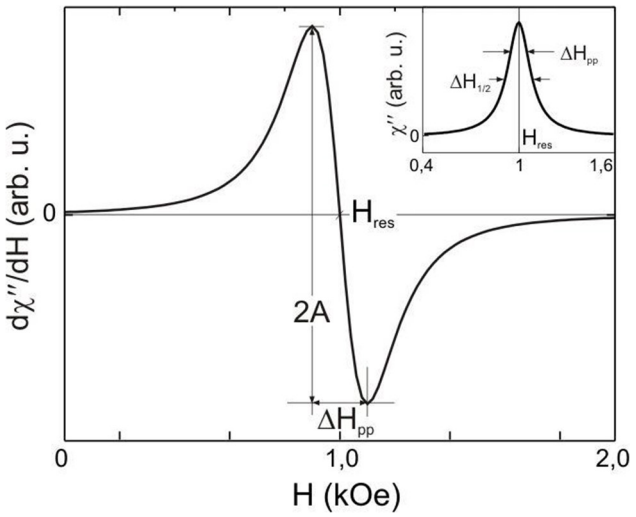

Figure 3. Derivative-like FMR absorption signal. The resonance field, H_{res}, depends on the g-factor, anisotropy as well as the magnetization of the sample. ΔH_{pp} is a measure of the magnetic damping [22].

[8] We note that with the definition for the quality factor of the unloaded cavity $Q_0 = 2\pi W_{\text{cav}}^{\text{store}}/W_{\text{loss}}^{\text{int}}$ and the external quality factor $Q_{\text{ext}} = 2\pi W_{\text{cav}}^{\text{store}}/W_{\text{loss}}^{\text{ext}}$ one obtains the relation $1/Q_L = 1/Q_0 + 1/Q_{\text{ext}}$. The coupling parameter $\beta = W_{\text{loss}}^{\text{ext}}/W_{\text{loss}}^{\text{int}} = Q_0/Q_{\text{ext}}$ which characterizes the energy loss in the external circuit in relation to the one inside the cavity then yields $Q_L = Q_0/(1+\beta)$. For the so-called critical coupling the internal cavity losses are equal to the coupling losses, or in other words, half the microwave power in the cavity reaches the electronics via the coupler, while the other half is dissipated in the cavity walls. In this case $\beta = 1$ and therefore $Q_L = Q_0/2$. This critical coupling is often assumed so that the term $Q_0/2$ appears in equation (3).

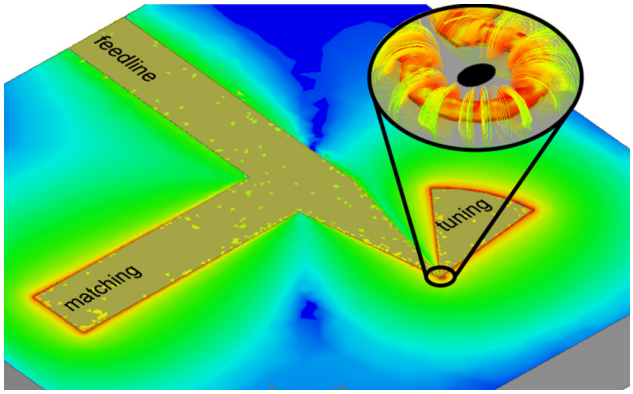

Figure 4. Layout of a planar microresonator with simulated electric field distribution at resonance frequency. The inset shows the current and magnetic field distribution in the loop containing a sample (black ellipse).

$$F = \frac{\int_{sample} h_{rf}^2 V_s}{\int_{cavity} h_{rf}^2 V_c} \approx \frac{V_s}{V_c}, \tag{4}$$

where h_{rf} is the microwave field, and V_{s} and V_{c} are sample and cavity volume, respectively. The filling factor can be approximated by the ratio of the sample to the cavity volume if the microwave field h_{rf} is homogeneously distributed.

In conventional approaches to detect magnetic resonance, samples are placed within cavities, whose minimal dimensions are defined by the half wavelength of the operation frequency. For the most popular X-band spectrometers (~10 GHz), the cavities are thus centimeters large. This limits the measurable sample volume to the order of typically mm^3, while at that size cavities can reach sensitivities of 10^{10} spins/$\mathrm{GHz}^{1/2}$ [21]. Detecting the FMR signal of nano-to micron-sized samples in conventional cavities is therefore not possible, due to their too small ferromagnetic volume. Planar microresonators were introduced by Narkowicz *et al* for electron paramagnetic resonance (EPR) experiments to achieve optimal sensitivity for small objects [25]. While the quality factor of planar resonators is two to three orders of magnitude lower than that of their bulk counterparts, they allow one to adjust the active detection volume to approach the actual sample size and thus increase the filling factor considerably. As a planar microresonator is by definition a 2D structure, the resonator extension into the third dimension is negligible. Moreover, the sample is placed within a loop, whose diameter can be tailored to match the order of the sample's size. Two stubs are attached to the inductive loop. The capacitive radial stub in first approximation may be viewed as element to tune the loop to the operation frequency, while the rectangular stub matches the structure to the 50 Ω impedance of the microstrip feedline (figure 4). In fact, either of the stubs influences both, tuning and matching of the resonator. At resonance, a standing wave establishes between the edges of the stubs, as can be seen in the snapshot of the electrical rf-field distribution simulation shown in figure 4. Due to small dimensions of the loop, the electric current density within the loop in the vicinity of the sample at resonance gets very high which leads to an efficient conversion of the excitation power into an out-of-plane microwave magnetic rf-field within the sample volume.

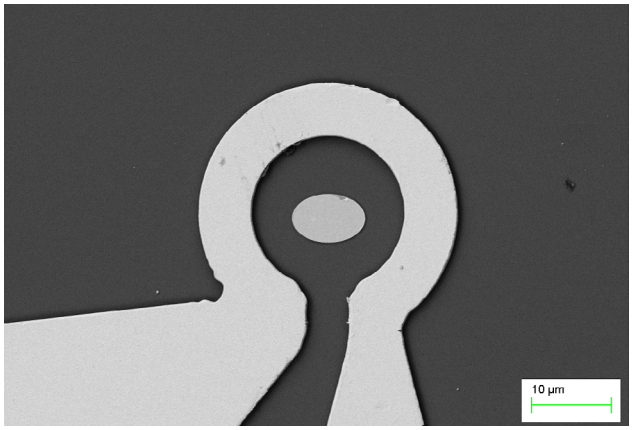

Figure 5. SEM image of MTJ integrated into 20 μm loop microresonator.

Therefore, the FMR signal from micro- and nanosized ferromagnetic samples can be detected with ultrahigh sensitivity.

2.2. Material preparation and laser heating system

We investigated magnetic tunnel junctions (MTJs), which were fabricated out of MgO/MgO(10)/TiN(30)/Co_2FeAl(10)/MgO(2)/CoFeB(3)/Ta(3)/Ru(3)/Cr(5)/Au(60) stacks, where the layer thicknesses in nm is given in parenthesis. The TiN-layer promotes an epitaxial growth of the Co_2FeAl(10)-film, while the Ta/Ru capping layer prevents the stack from oxidation. We additionally deposited a 60 nm thick Au-film on top to act as absorption layer for the laser light. It was recently shown that using Co_2FeAl as reference layer improves the TMS effect in MTJs [32]. After deposition, the samples were annealed under the presence of an in-plane magnetic field of 0.7 T at 325 °C for 1 h. Broadband FMR was used on the extended films to characterize their dynamical properties. The sample and microresonator fabrication consists of multiple steps such as lithography, ion etching and lift-off processes. The sample is finally patterned into a 6×9 $\mu\mathrm{m}^2$ elliptical shape pillar using electron beam lithography (EBL), and ion beam etching to etch down the sample to the substrate. Microresonators are then fabricated around the sample using UV lithography. An MTJ incorporated into a microresonator is shown by an SEM image in figure 5. The metallization of the microresonator was performed using e-beam evaporation. Our experimental approach is to observe the FMR response of the MTJ structures under application of thermal gradients across their barriers. We thus established a microresonator FMR setup, where a laser beam can be focused onto the sample in order to heat the sample stack from the top. The sketch of the experimental setup is shown in figure 6(a). A Laser diode (Thorlab) at 638 nm wavelength and with tunable power up to 200 mW (calibrated value is 145 mW) is focused to the sample. An electromagnet produces a stable and homogenous DC field parallel to the film plane, while the micro-coil generates an ac magnetic field perpendicular to the film plane (figure 6(b)). We used the microwave bridge detection as described above in order to measure the sample in reflection geometry with higher signal-to-noise ratio (SNR) by using field modulation and lock-in detection.

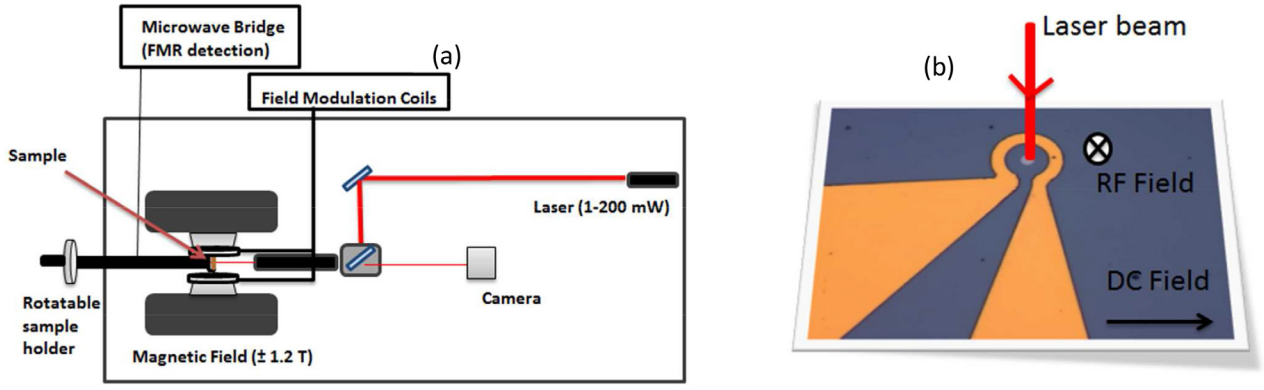

Figure 6. (a) Sketch of the experimental setup to detect FMR signal under laser heating. (b) Sketch of the experimental approach to detect FMR signals of the samples using microresonator.

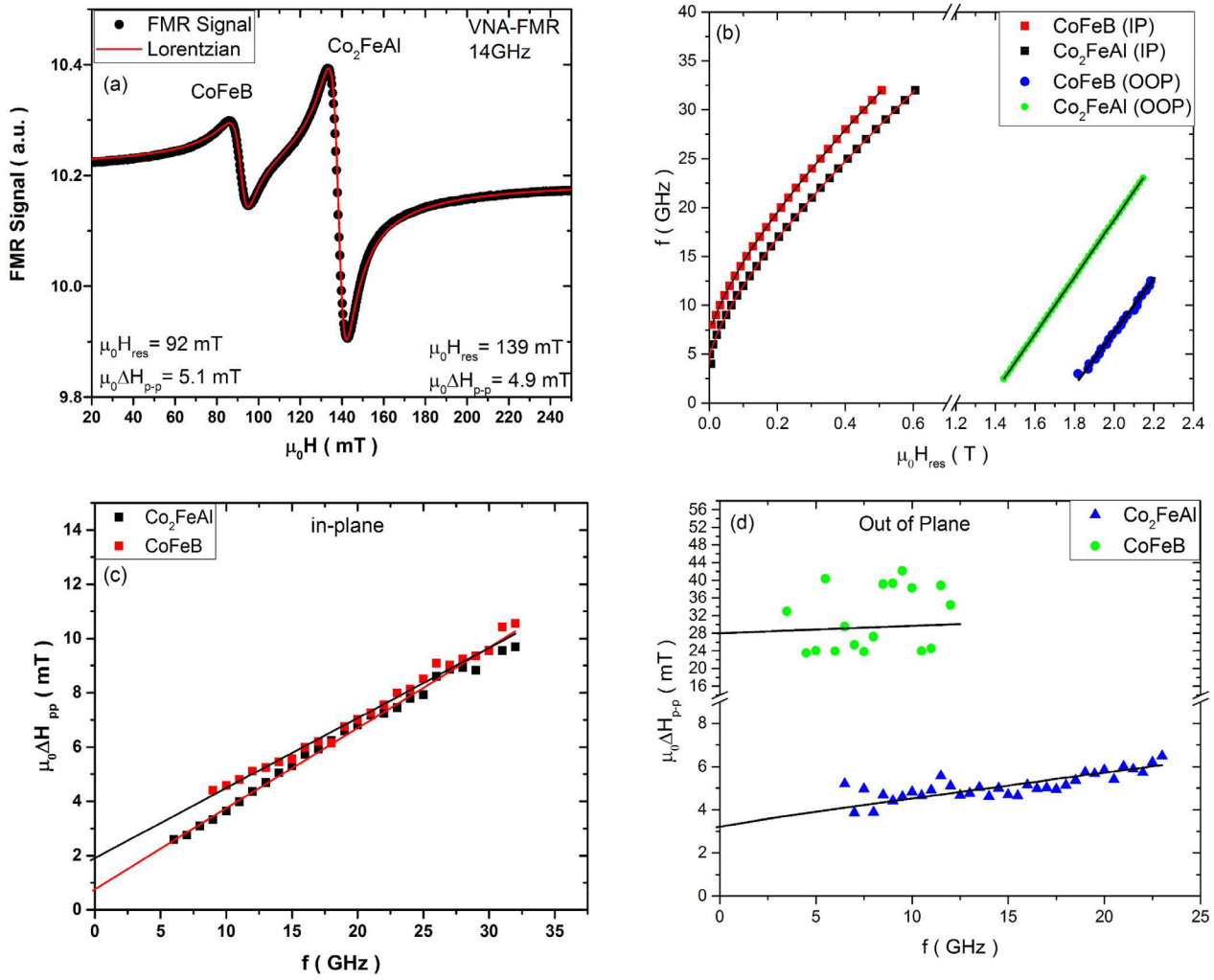

Figure 7. (a) Single VNA-FMR spectra taken at 14 GHz. (b) Field dependence of resonance frequency for CoFeB and Co_2FeAl for in-plane and out of-plane field orientations (solid lines are fits to the data). Linewidth dependence of resonance frequency for CoFeB and Co_2FeAl for (c) in-plane and (d) out of-plane field orientation.

3. Results and discussion

3.1. Broadband ferromagnetic resonance on extended thin film systems

Before performing experiments under laser irradiation, we performed broadband vector network analyzer (VNA) FMR measurements on extended films to identify the dynamic properties of the two ferromagnetic layers within the stack. The results are summarized in figure 7. Figure 7(a) shows a single VNA-FMR spectrum taken at 14 GHz which is the operating frequency of our microresonators. One can clearly identify the two signals of the Co_2FeAl and the CoFeB layers, the latter being located at smaller resonance fields, due to the

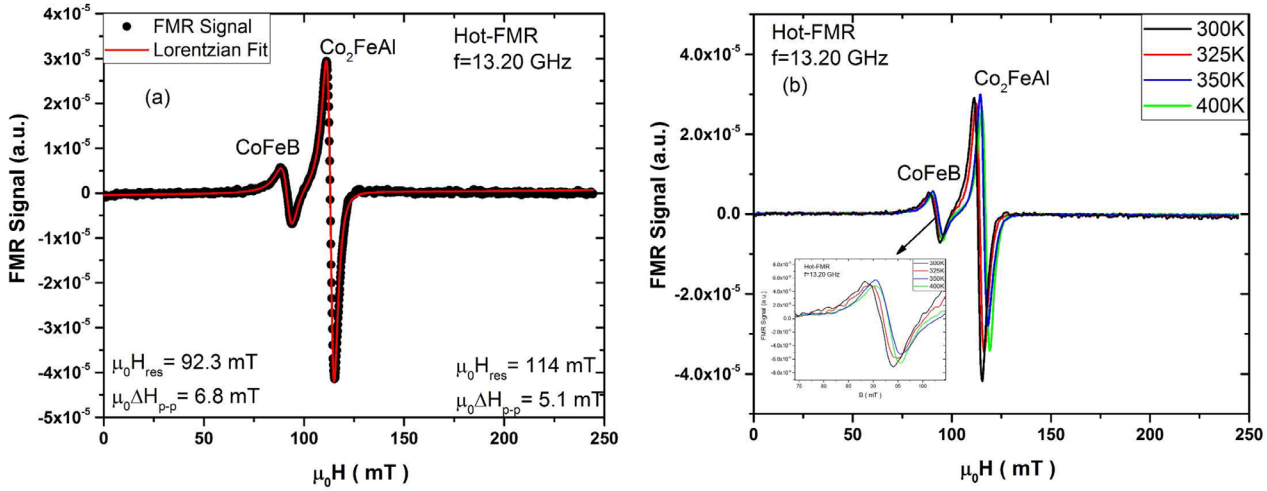

Figure 8. (a) FMR spectra of the extended sample measured at RT at 13.20 GHz. (b) FMR spectra of the extended film measured in the in-plane direction at different temperatures.

fact that CoFeB exhibits a larger magnetization. The films exhibit a significant cubic in-plane anisotropy which is not the focus of this paper. We only note that all our experiments (VNA-FMR as well as microresonator FMR) were carried out with external field parallel to the easy in-plane direction, or in the geometry for which the external field is perpendicular to the layer planes. From the fitting of both resonance field with a complex Lorentzian function, we extracted the resonance field and the linewidth of both signals, whereby we used microwave frequencies in the range 3–32 GHz. The obtained resonance fields for the different frequencies are plotted in figure 7(b) for the external magnetic field being applied in-plane (squares), as well as out-of-plane (circles). The solid lines are fits for the Co_2FeAl (black/green) and CoFeB (red/blue), data according to the resonance equations [36]. The effective magnetization, $4\pi M_{\text{eff}}$, and the g-factor are considered as fitting parameters. The fitted g-value is found to be around $g = 2.086 \pm 0.002$ for both layers, consistent with literature [34]. The saturation magnetization values, M_s, determined from vibrating sample magnetometry (VSM), are very close to the effective magnetization, determined by FMR, i.e. the value of the perpendicular anisotropy contributing to $4\pi M_{\text{eff}}$ is negligible. The values for $4\pi M_{\text{eff}}$ are found to be 1.305 ± 0.01 T for Co_2FeAl and 1.619 ± 0.001 T for CoFeB. From the VSM results, the M_s values are 1.28 ± 0.01 MA/m for Co_2FeAl and 1.62 ± 0.01 MA/m for CoFeB. We note that the VSM experiments were performed on individual extended films of Co_2FeAl (5) and CoFeB (5) and are not shown here. From the VNA-FMR data, we also extracted the linewidth as function of frequency for both the Co_2FeAl and CoFeB layers in the in-plane and out-of-plane direction as shown in figures 7(c) and (d). The linewidths for Co_2FeAl and CoFeB show a linear dependence on frequency. The CoFeB data shows more scattering, as the CoFeB signal is weaker than the signal of the Co_2FeAl. The Gilbert damping of Co_2FeAl (CoFeB) is determined to be $\alpha = 0.0078 \pm 0.0001$ (0.007 ± 0.001) for the in-plane and $\alpha = 0.003 \pm 0.001$ (0.004 ± 0.0034) along the out-of-plane directions, with an inhomogeneous broadening of $\Delta\mu_0 H_0 = 0.7$ mT (1.9 mT) and $\mu_0 H_0 = 3.1$ mT (28 mT), respectively. The reason for the slightly higher in-plane damping for the Co_2FeAl-layer might be attributed to an additional damping contribution, which is less effective for the out-of-plane geometry. We rule out two-magnon scattering, as such a contribution, because of the linear, Gilbert-like dependence for the in-plane direction. As the CoFeB layer is on top of the stack and therefore subject to increased roughness and imperfection, we observe a larger inhomogeneous broadening. Note that the low frequency increase of the Co_2FeAl linewidth might result from a slight misalignment of the external field along the hard out-of-plane axis.

3.2. Temperature-dependent FMR on extended films

To investigate the effect of global heating, FMR measurements were performed on unpatterned multilayers between 300 K and 400 K. For this, the sample was mounted on a ceramic heater with a Pt100-thermoelement for temperature measurements. For the microwave excitation and FMR detection, a semi-rigid cable with an SMP connector was placed just a few hundred micrometers above the surface of the film [38]. The whole sample holder is located inside a quartz glass tube, which can be evacuated to avoid oxidation during heating. The assembly was then mounted between the pole caps of an electromagnet, which is equipped with additional modulation coils. For the FMR detection, the same type of microwave bridge as for the microresonator setup was used.

First, the FMR spectrum was measured at room temperature as shown in figure 8(a) with a corresponding Lorentzian fit (solid line). The FMR spectrum shows the signals corresponding to the two ferromagnetic layers. Note that the slightly smaller resonance field as compared to the VNA-FMR spectrum in figure 7(a) results from the somewhat smaller frequency (13.20 GHz). In figure 8(b), FMR spectra at different temperatures are shown. It is clearly seen that the FMR signal of Co_2FeAl exhibits a shift with increasing temperature. As seen in the inset graph, the CoFeB signal also shifts to higher resonance fields by increasing the temperature.

3.3. Ferromagnetic resonance in microresonator

Measurements in the presence of a thermal gradient were performed on 6×9 μm^2 MTJs, integrated into microresonator loops with an inner diameter of 20 μm. The MTJs were exposed to laser radiation, with the power increasing from 0 to 145 mW. The spot size of the laser beam was around 5 μm, thus smaller than the lateral size of the MTJ. In figure 9(a), an FMR spectrum measured at 13.73 GHz (which corresponds to the optimum sensitivity of the microresonator) is shown for the case when the laser is off. A Lorentzian fit (solid red line) is used to determine the resonance field and the linewidth. Again, one can clearly identify the signals of the CoFeB and the Co_2FeAl layers.

In addition to laser-based experiments, we performed global heating investigations on a structured sample. For this, a current-driven heater element was mounted on the backside metallization of the microresonator chip, while the temperature was measured by a thermoelement whose voltage was fed into a controller. We used the same structured sample as for the global heating study; however, a different FMR magnet had to be used, having a larger gap between the poles to be able to fit the heater in. Contrary to the laser-based magnet, setup where the in-plane angle of the external dc-field was adjusted to match the easy axis of the sample, did not allow for a similarly accurate adjustment in the setup used for global heating. Consequently, we cannot fully rule out small angular misalignments between the two setups (about 1–2°).

To estimate the induced global temperature rise, as well as the small temperature gradient resulting from the laser heating, we performed COMSOL simulations using its heat transfer module. The heat diffusion problem is modeled by starting with a 2D (vertical) rectangular shape in which we consider the MTJ stack with the MgO-substrate below. Aside the MTJ we consider an air layer on top of the MgO-substrate. Upon rotation of this two-dimensional shape around the central vertical axis of the MTJ, we obtain a 3D cylinder in which the heat profile is simulated. The simulation parameters for the materials were chosen similar to those in [14]. The inset of figure 3(d) shows the result of the obtained temperature profile, indicating that at the maximum laser power (of 145 mW) we achieve a temperature gradient of about 400 mK. Moreover, the simulations allow toconvert the laser power into a global temperature, which can be then compared to our experiments using a global heating procedure as described above. We note that this conversion becomes necessary, since influences on the resonance field due to the thermal gradient cannot be excluded due to a possible out-of-plane torque which would directly act on the frequency of the precession, thus influencing the resonance field.

Since the changes to magnetization dynamics induced by thermal torques affect mostly the free layer, we focus in the following on the signal CoFeB. At this point we want to mention that due to the operation frequency of our resonators, requiring resonance fields larger than the coercivity of both layers, we can only investigate the system after exciting small-angle precession close to the parallel state. The resonance field and linewidth changes of the CoFeB-signal are shown as a function of temperature in figures 9(b) and (c), respectively. As seen in figure 9(b), the resonance field clearly increases with temperature for the extended film (black squares) as well as for the structured film under global heating (blue circles). In contrast, the resonance field of the structured sample (red circles) under laser heating exhibits only a slight increase (see inset with magnified resonance field axis for clarity). One observes a decrease of the resonance field due to the structuring the sample into the elliptical shape. This results from the extra in-plane anisotropy, generated due the asymmetric shape. As the long axis of the ellipse was chosen to be aligned parallel to the easy direction of the CoFeB, the easy-axis character is enhanced, leading to smaller resonance fields. The small deviation between the resonance field of the structured sample at 300 K when globally heated or laser heated might result from the above-mentioned misalignment errors which are intrinsic to the use of two different setups. The linewidth of the structured sample behaves qualitatively very different as compared to global heating condition (see figure 9(c)). A decrease in linewidth with temperature is observed for the extended film as well as the structured sample when globally heated. On the contrary, the structured sample under laser heating shows a clear increase of the linewidth.

To explain the observed behavior, at first we note that a decreasing linewidth in thin film samples can be well understood in the context of temperature-dependent Gilbert damping, which is for many systems dominated by a conductivity-like contribution at low temperatures. This decreases towards higher temperatures, where a resistivity-like contribution takes over, leading to an increase of Gilbert damping [35]. We thus assume that (in our case) for room temperature we are located in a regime of dominating conductivity-like damping that decreases with temperature[9]. The fact that the laser heating leads to an increase of the linewidth, as compared to the global heating, indicates the presence of an extra torque that leads to an overall increase of damping. Because the only difference between the two heating procedures is the presence of a thermal gradient for the laser heating, we conclude that the relative linewidth increase (compared to the global heating) directly stems from a damping-like thermal torque. The fact that the difference between the linewidth observed for the two heating procedures increases with increasing global temperature proves this statement.

Coming back to the behavior of the resonance field, one would tend to argue in a similar manner, i.e. the increasing deviation with increasing global temperature between the resonance field measured for the global heating and laser heating, can be interpreted as being the result of (in this case) a field-like torque, which affects the precession frequency and thus the resonance field when using a constant measurement frequency as done in our microresonator approach. However, this torque seems to be surprisingly large (about 6 mT field shift at the highest temperature). Keeping in mind

[9] Note that we use linewidth and damping as synonyms, since we have found the Gilbert-damping to be dominant in our layers (see figures 7(c) and (d)), which allows one to identify an increase in linewidth as increase in Gilbert damping without the need to perform a full frequency dependent investigation of the linewidth.

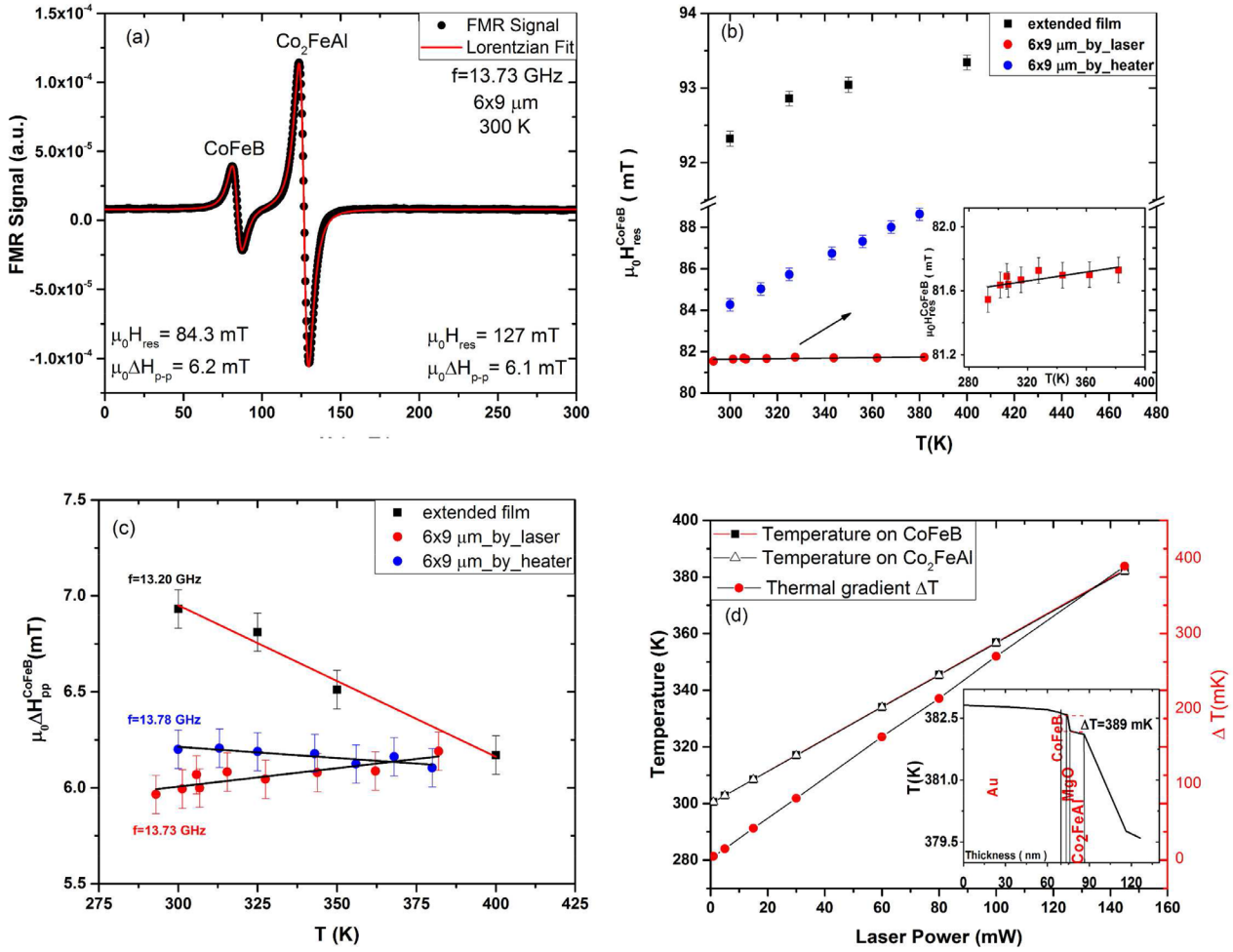

Figure 9. (a) FMR spectra of a micron-sized MTJ, incorporated into a 20 μm loop of a microresonator operating at 13.73 GHz. (b) The resonance field and (c) linewidth versus temperature are shown. (d) Temperature versus laser power obtained by COMSOL simulation, inset graph in (d) is the temperature profile across the MTJ with the power of 145 mW.

that at our microwave powers (at maximum 100 μW) we are well in the linear small-angle precession regime (precession angle at most 1°), this high value is likely to be affected by other factors as well. As such, we identified the above-mentioned potential misalignment between the external field and the CoFeB layer anisotropy in the setup. From the in-plane angular dependence of the resonance field measured for the thin film (not shown here) and assuming a misalignment of just 2°, one easily could explain resonance field shifts of about 1 mT. Moreover, the COMSOL simulations likely overestimate the global temperature of the MTJ. We found that the inclusion of the Cu loop around the sample in the simulations led to a significant reduction of the global temperature due to an effective heat transport away from the MTJ because of the Cu. We can, however, not exclude that the actual structure of the microresonator (which has not been considered in the simulation) leads to a further reduction in temperature. We note that such a further reduction would not change the qualitative statement, that we observe an increase of the linewidth in the laser heating experiment. On the contrary, in case that the actual temperature would be smaller, the increase in linewidth would be even more pronounced.

4. Conclusion and outlook

In this study, we described a novel experimental approach and setup to observe effects of thermal gradients within MTJs by using FMR microresonators. This approach allows for the detection of magnetization dynamics in 'open-circuit' condition, i.e. without the need of electrical contacts. Our experiments on mesoscopic samples show a significant influence of the laser irradiation on the linewidth and resonance field of the CoFeB free layer, as compared to the case where the whole sample is globally heated. This demonstrates that the thermal gradient leads indeed to a thermal spin-torque which acts on the free layer's magnetization. We observe two torque-contributions, damping-like torque as well as a field-like. Furthermore, we find that—upon exciting one layer and making it precess around the parallel state—the damping-like torque act to restore the parallel alignment of the two ferromagnetic layers ('extra' damping), while the field-like torque acts to increase the precession frequency. As we sweep the external magnetic field at constant frequency, the latter effect induces a reduction of the resonance field as compared to global heating. In our experiments, the thermal torques are well below required to induce switching. Nevertheless, we

observe clean signatures which can be used to quantify the magnitude of T-STT. Therefore, we consider this approach to be useful for studies in the low thermal gradient regime, which so far was proven to be the case in most investigated studies.

Acknowledgment

This study was funded by the German Research Foundation (DFG) via priority program SpinCaT (SPP 1538). Support by the Nanofabrication Facilities Rossendorf at IBC is gratefully acknowledged. We thank H Schultheiß for helping with the optical part of the experimental setup and S Zhou for support of the VSM measurements.

ORCID iDs

H Cansever https://orcid.org/0000-0003-0595-4949
T Huebner https://orcid.org/0000-0003-4813-4270

References

[1] Johnson M and Silsbee R H 1987 *Phys. Rev.* B **35** 4959
[2] Bauer G E W, Saitoh E and van Wees B J 2012 *Nat. Mater.* **11** 391
[3] Uchida K, Takahashi S, Harii K, Ieda J, Koshibae W, Ando K, Maekawa S and Saitoh E 2008 *Nature* **455** 778
[4] Jansen R 2012 *Nat. Mater.* **11** 400
[5] Hatami M, Bauer G E W, Zhang Q and Kelly P J 2007 *Phys. Rev. Lett.* **99** 066603
[6] Yu H, Granville S, Yu D P and Ansermet J-Ph 2010 *Phys. Rev. Lett.* **104** 146601
[7] Jia X, Xia K and Bauer G E W 2011 *Phys. Rev. Lett.* **107** 176603
[8] Liebing N, Serrano-Guisan S, Rott K, Reiss G, Langer J, Ocker B and Schumacher H W 2011 *Phys. Rev. Lett.* **107** 177201
[9] Leutenantsmeyer J C *et al* 2013 *Spin* **3** 1350002
[10] Boehnke A *et al* 2015 *Sci. Rep.* **5** 8945
[11] Liebing N, Serrano-Guisan S, Rott K, Reiss G, Langer J, Ocker B and Schumacher H W J 2012 *Appl. Phys.* **111** 07C520
[12] Shan J, Dejene F K, Leutenantsmeyer J C, Flipse J, Münzenberg M and van Wees B J 2015 *Phys. Rev.* B **92** 020414
[13] Walter M *et al* 2011 *Nat. Mater.* **10** 742
[14] Huebner T, Boehnke A, Martens U, Thomas A, Schmalhorst J M, Reiss G, Münzenberg M and Kuschel T 2016 *Phys. Rev.* B **93** 224433
[15] Zhang Z, Bai L, Chen X, Guo H, Fan X L, Xue D S, Houssameddine D and Hu C-M 2016 *Phys. Rev.* B **94** 064414
[16] Wigen P E, Kooi C F, Shanaberger M R and Rosing T R 1962 *Phys. Rev. Lett.* **9** 206
[17] Vonsovskii S V 1966 *Ferromagnetic Resonance* (Oxford: Pergamon)
[18] Wigen P E and Zhang Z 1992 *Braz. J. Phys.* **22** 267
[19] Farle M 1998 *Rep. Prog. Phys.* **61** 755
[20] Fermin J R, Azevedo A, Aguiar F M, Li B and Rezende S M J 1999 *Appl. Phys.* **85** 7316
[21] Poole C P Jr 1967 *Electron Spin Resonance* (New York: Interscience)
[22] Lenz K 2005 *PhD Thesis* Freie Universität Berlin
[23] Banholzer A, Narkowicz R, Hassel C, Meckenstock R, Stienen S, Posth O, Suter D, Farle M and Lindner J 2011 *Nanotechnology* **22** 295713
[24] Boero G, Bouterfas M, Massin C, Vincent F, Besse P-A, Popovic R S and Schweiger A 2003 *Rev. Sci. Instrum.* **74** 4794
[25] Narkowicz R, Suter D and Stonies R 2005 *J. Magn. Reson.* **175** 275
[26] Möller M, Lenz K and Lindner J 2014 *J. Surf. Interfac. Mater.* **2** 46
[27] Slonczewski J C 1996 *J. Magn. Magn. Mater.* **159** L1
[28] Berger L 1996 *Phys. Rev.* B **54** 9353
[29] Onsager L I 1931 *Phys. Rev.* **37** 405
[30] Landau E, Lifshitz E and Physik Z 1935 *Sowjetunion* **8** 153
[31] Deac A M, Fukushima A, Kubota H, Maehara H, Suzuki Y, Yuasa S, Nagamine Y, Tsunekawa K, Djayaprawira D D and Watanabe N 2008 *Nat. Phys.* **4** 803
[32] Boehnke A *et al* 2017 *Nat. Commun.* **8** 1626
[33] Poole Ch P and Farach H A 1999 *Handbook of Electron Spin Resonance*
[34] Liu X, Zhang W, Carter M J and Xiao G J 2011 *Appl. Phys.* **110** 033910
[35] Gilmore K, Stiles M D, Seib J, Steiauf D and Fähnle M 2010 *Phy. Rev.* B **81** 174414
[36] Liedke M O *et al* 2013 *Phys. Rev.* B **87** 024424
[37] Ralph D C and Stiles M D 2008 *J. Magn. Magn. Mater.* **320** 1190
[38] Römer F M *et al* 2012 *Appl. Phys. Lett.* **100** 092402